SCIENTIFIC REPORTS

OPEN

SUBJECT AREAS:
QUANTUM DOTS
SOLAR CELLS
OPTICAL MATERIALS
NANOPARTICLES

Received
10 October 2012

Accepted
17 December 2012

Published
10 January 2013

Correspondence and requests for materials should be addressed to N.-G.P. (npark@skku.edu)

Quantum-Dot-Sensitized Solar Cell with Unprecedentedly High Photocurrent

Jin-Wook Lee[1], Dae-Yong Son[1], Tae Kyu Ahn[1], Hee-Won Shin[1], In Young Kim[2], Seong-Ju Hwang[2], Min Jae Ko[3], Soohwan Sul[4], Hyouksoo Han[4] & Nam-Gyu Park[1]

[1]Department of Energy Science, School of Chemical Engineering, Sungkyunkwan University, Suwon 440-746, Korea, [2]Center for Intelligent Nano-Bio Materials (CINBM), Department of Chemistry and Nano Sciences, Ewha Womans University, Seoul 120-750, Korea, [3]Photo-Electronic Hybrids Research Center, Korea Institute of Science and Technology (KIST), Seoul 136-791, Korea, [4]Center for Computer Simulation and Analytical Science, Samsung Advanced Institute of Technology (SAIT), Yongin 446-712, Korea.

The reported photocurrent density (J_{SC}) of PbS quantum dot (QD)-sensitized solar cell was less than 19 mA/cm^2 despite the capability to generate 38 mA/cm^2, which results from inefficient electron injection and fast charge recombination. Here, we report on a PbS:Hg QD-sensitized solar cell with an unprecedentedly high J_{SC} of 30 mA/cm^2. By Hg^{2+} doping into PbS, J_{SC} is almost doubled with improved stability. Femtosecond transient study confirms that the improved J_{SC} is due to enhanced electron injection and suppressed charge recombination. EXAFS reveals that Pb-S bond is reinforced and structural disorder is reduced by interstitially incorporated Hg^{2+}, which is responsible for the enhanced electron injection, suppressed recombination and stability. Thanks to the extremely high J_{SC}, power conversion efficiency of 5.6% is demonstrated at one sun illumination.

Quantum dot (QD, semiconductor nanocrystal) has been recently drawing great attention as a material for solar energy conversion due to high absorption coefficient, tunable band gap and multiple exciton generation (MEG) effect[1–4]. QDs have been actively studied in dye-sensitized solar cell (DSSC) as alternatives to conventional organic dyes[5]. As a result, remarkable accomplishments have been achieved in recent year, where a power conversion efficiency (PCE) of ca. 5% was achieved using metal chalcogenides[6,7] and around 10% using organic-inorganic perovskite[8]. However, most of the studied QDs for DSSC were based on the relatively large band gap materials (>1.5 eV)[6–8]. Using these materials, it may not be possible to utilize the full solar spectrum, which leads to a limited short-circuit photocurrent density (J_{SC}) of ca. 20 mA/cm^2 (considering 20% loss from FTO glass)[9]. No successful examples have been reported on high J_{SC} QD-sensitized solar cells based on low band gap QDs (<1.5 eV) although it has ability to generate extremely high J_{SC} owing to near IR absorption.

Among the various low band gap QDs, PbS is one of the most intensively studied low band gap semiconductors since it has a high absorption coefficient of $1\sim5\times10^5$ cm^{-1} and wide range of tunable band gap owing to its large bohr exciton radius of 18 nm[10,11]. There have been a lot of efforts to use the PbS QD as a sensitizer. Antonio Braga *et al.* demonstrated a PCE of 2.21% with J_{SC} of 10.91 mA/cm^2 using PbS/CdS QD photoelectrode being in contact with polysulfide electrolyte[12]. Very recently, it was enhanced to 3.82% with J_{SC} of 18.84 mA/cm^2 by incorporating PbS/CdS QD in hierarchical porous TiO_2[13]. However, the observed J_{SC}s are still far below the theoretical value of 38 mA/cm^2 (after considering 20% light reflection at FTO) when considering the band gap of ca. 1.0 eV[9].

Main drawback of PbS QD in QD-sensitized solar cell has been argued to be inefficient charge separation and collection due to slow electron transfer kinetics[14]. Electron injection from the conduction band of PbS QD to the conduction band of TiO_2 was measured to be a ca. 100 ns, which is five times slower than CdSe QD (20 ns from colloidal in organic solvent)[14]. In addition, it was also argued that PbS QD served as critical recombination center, which means that injected electrons in conduction band of TiO_2 tends to recombine readily with positively charged PbS QD, and thereby efficient charge collection was seriously impeded[12,15]. For efficient charge separation and collection from the PbS QD, injection and recombination kinetics of PbS QD must be tuned. However, little attempt has been made to date.

Here, we report on a QD-sensitized solar cell with J_{SC} approaching 30 mA/cm^2 based on PbS:Hg QDs. Deposition of PbS:Hg QD on nanostructured TiO_2 is implemented by simple wet chemical process, where the photovoltaic performance is evaluated by using polysulfide as a redox electrolyte. Noticeable conversion efficiency of 5.6% with unprecedented high J_{SC} is demonstrated under AM 1.5G one sun illumination. Electron injection and charge recombination kinetics are studied by femtosecond transient absorption measurements.

Chemical bonding nature surrounding Pb and Hg is investigated by extended X-ray absorption fine structure (EXAFS).

Results

Fig. 1a shows deposition process of PbS:Hg QD on nanostructured TiO_2 surface using successive ionic layer adsorption and reaction (SILAR) method. Pb^{2+} and Hg^{2+} ions are adsorbed on TiO_2 surface during the first dipping, which is followed by chemical reaction with S^{2-} ion in second bath to form PbS:Hg QD on TiO_2 surface. Concentration of $HgCl_2$ is varied from 0 mmol to 8 mmol to evaluate the effect of Hg^{2+} concentration. Fig. 1b shows TEM micrographs of bare TiO_2 and PbS:Hg QD-adsorbed TiO_2 with different $HgCl_2$

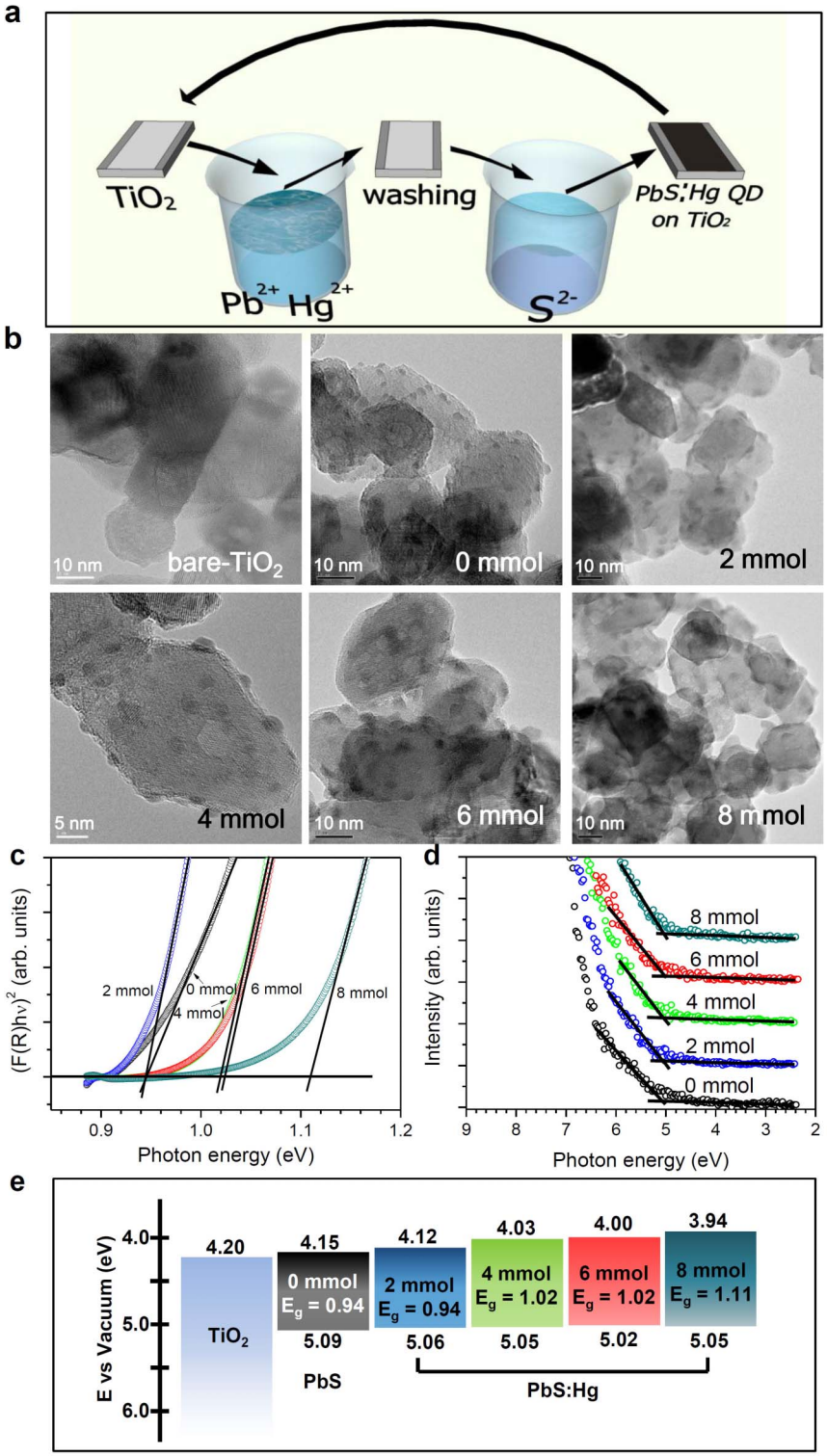

Figure 1 | Morphology and energetic properties of PbS and PbS:Hg QDs. (a) Deposition process of PbS:Hg QDs on mesoporous TiO_2 nanostructure using successive ionic layer adsorption and reaction (SILAR) method. (b) TEM micrograph of bare TiO_2 and QD coated TiO_2 nanoparticles using the cationic solution containing 0 mmol, 2 mmol, 4 mmol, 6 mmol and 8 mmol of $HgCl_2$. (c) Tauc plot calculated by using Kubelka-Munk equation from reflectance spectra. (d) UPS spectra of PbS:Hg QD adsorbed TiO_2 and extrapolation of low binding energy region. (e) Band edge alignment diagram for PbS and PbS:Hg QDs.

concentration. It is clearly identified that semi-sphered QDs are sparsely formed on the surface of TiO_2 nanoparticles regardless of $HgCl_2$ concentration. Pb L3 and Hg L3 edges X-ray absorption near edge spectroscopy (XANES) spectra of bulk PbS and HgS with PbS:Hg QDs deposited on TiO_2 nanoparticles are compared in Supplementary Fig. S1. To identify undesired impurity species, PbO, PbO_2, $Pb(NO_3)_2$ and $HgCl_2$ are also measured as references. All electrodes showed almost identical shape with bulk PbS and HgS, which means that lead and mercury ions in samples exist in the form of Pb^{2+} and Hg^{2+} bonded to S^{2-} [16,17]. Since it was reported that the peak area in X-ray photoelectron spectroscopic (XPS) data, representing the number of electrons, is assumed to be proportional to the number of atoms in a given state[18], the doping concentration is estimated from the area of Pb 4f and Hg 4f peaks (Supplementary Fig. S2, Table S1). As expected, the ratio of Hg^{2+} to (Pb^{2+} + Hg^{2+}) increases as the $HgCl_2$ concentration increases. Doping concentration of Hg^{2+} in PbS:Hg is estimated to be 0, 5.4, 6.3, 14.6 and 16.7 at% for 0, 2, 4, 6 and 8 mmol of $HgCl_2$, respectively. Relatively high amount of Hg content of 16.7 at% for 8 mmol compared to the nominal composition (7.4 at%) is due to the stronger oxidizing characteristic of Hg^{2+} than Pb^{2+} [19].

Optical band gap of the QDs is estimated from reflectance spectra using Kubelka-Munk equation[20] and Tauc plot[21] (Fig. 1c). The optical band gap of PbS:Hg QD increases from 0.94 eV to 1.11 eV as the doping concentration increases from 0 at% to 16.7 at%. UV-vis absorption spectra of PbS:Hg QDs look red-shifted compared to the pristine PbS, especially in visible region as can be seen in Supplementary Fig. S3a. However, the threshold for the PbS doped with Hg (equal or greater than 4 mmol) in the NIR region in inset of Fig. S3a is moved to shorter wavelength than the pristine PbS, which is consistent with the increase in band gap. From the detailed investigation on $HgCl_2$ concentration change from 0 mmol to 2 mmol and from 4 mmol to 6 mmol, optical band gap is almost unchanged in spite of the increased Hg^{2+} in PbS:Hg, which is related to quantum size effect (ca. 2.4 nm for 0 mmol, ca. 4.0 nm for 2 mmol and 4 mmol, and ca. 5.7 nm for 6 mmol and 8 mmol) as can be seen in Supplementary Fig. S4. As mentioned before, increase in Hg doping concentration is expected to enlarge the optical band gap, which, however, will be compensated with increase in QD size. For this reason, little change in band gap is observed between 0 mmol and 2 mmol or 4 mmol and 6 mmol. Valence band maximum (VBM) is determined by ultraviolet photoelectron spectroscopy (UPS)[22]. Secondary cut-off is fitted to energy of He I light source (21.2 eV), where extrapolation of low energy region corresponds to potential energy of VBM from the vacuum level (Fig. 1d)[22]. It is noted that VBM is hardly changed by Hg concentration, which indicates that VBM is mainly dominated by S ion. The position of conduction band minimum (CBM) is calculated based on VBM and optical band gap energy. Band edge alignment is demonstrated in Fig. 1e, where CBMs of the QDs move upward as the concentration of $HgCl_2$ increases, leading to gradual increase in optical band gap. PbS doped with Hg is measured to be p-type semiconductor (Supplementary Table S2), where thin film of PbS:Hg deposited on glass substrate is used for the Hall measurement instead of using QD-adsorbed TiO_2 film because deposited QD on TiO_2 is discontinuous.

Photovoltaic performances of PbS:Hg QD-sensitized solar cells are evaluated from current density-voltage (J-V) and external quantum efficiency (EQE) measurements (Fig. 2). Schematic structure of the QD-sensitized solar cell is depicted in Fig. 2a. Dependence of photovoltaic performance on the SILAR coating cycle number is first investigated at the given TiO_2 thickness of 6.5 μm (Supplementary Fig. S5). Optimum coating cycle for best efficiency is found to be 2 cycles for PbS (0 mmol of $HgCl_2$), 4 cycles for both 2 mmol and 4 mmol $HgCl_2$ and 6 cycles for both 6 mmol and 8 mmol $HgCl_2$ (Supplementary Fig. S5 and S6 and Table S3). In case of 0 mmol $HgCl_2$ condition (PbS), efficiency reaches maximum at 2 coating cycles (Supplementary Fig. S6a) although absorption is further increased after 2 cycles (Supplementary Fig. S7a). This might be related to decreased band gap due to large sized PbS QD formed after several coating cycles[14] (ca. 5.7 nm for 6 cycle in Supplementary Fig. S4). No further increase in short-circuit current density (J_{SC}) is observed after 2 coating cycle (Supplementary Fig. S6b). On the other hand, PbS:Hg (2∼8 mmol $HgCl_2$) shows significant increase in J_{SC} as the coating cycle is increased, which is due to the increased absorption (Supplementary Fig. S6b and Fig. S7b). Fig. 2b shows J-V curves of the PbS:Hg QD-sensitized solar cells depending on $HgCl_2$ concentration and photovoltaic parameters are summarized in Table S4, where ca. 10 μm-thick TiO_2 film is used since optimal efficiency is obtained with around 10 μm-thick film from the investigation on dependence of TiO_2 film thickness on photovoltaic performance (Supplementary Fig. S8 and Table S5). J_{SC} of QD-sensitized solar cell is substantially improved after Hg^{2+} doping. By adding 2 mmol of $HgCl_2$ in Pb^{2+} precursor solution, conversion efficiency is significantly improved from 2.38% to 3.78%, which is mainly due to remarkable increase in J_{SC} from 13.68 mA/cm^2 to 22.27 mA/cm^2 (63% increment). For the case of Hg^{2+} doped PbS, as the concentration of $HgCl_2$ increases from 2 mmol to 8 mmol, no significant change in J_{SC} is observed, whereas V_{OC} is gradually increased. Since the fill factors are degraded as photocurrent increase, shunt and series resistances are calculated from slope of J-V curves at short-circuit and at open-circuit region, respectively, using K2400 I-V system program based on LABVIEW (PV Measurements Inc) and plotted in Supplementary Fig. S9. Change in shunt resistance and series resistance are investigated as function of TiO_2 film thickness and number of coating cycle. Upon increasing TiO_2 film thickness or number of coating cycle, photocurrent is increased, while both shunt and series resistances are decreased. As can be seen in Tables S3 and S5, fill factors are decreased with increasing TiO_2 film thickness or number of coating cycle, which is due to the decreased shunt resistance despite the decreased series resistance.

EQE spectra are demonstrated in inset of Fig. 2b. Maximum EQE of PbS:Hg QD sensitized solar cell reaches 74.6% at 470 nm, which is improved by 78% compared to the maximum EQE of 41.8% at 400 nm for PbS QD sensitized one. EQE is substantially enhanced from visible to near IR region, where 123% at 500 nm (from 33.1% to 74%), 472% at 700 nm (from 9.41% to 53.8%) and 440% at 1000 nm (from 1.89% to 10.2%) are improved. Stability of the devices is evaluated by measuring J_{SC} with respect to time after electrolyte injection (Fig. 2c). J_{SC} of PbS QD sensitized solar cell sharply decreases immediately after electrolyte injection, where almost 80% of J_{SC} degrades during the initial 180 seconds. Instability of PbS QD in polysulfide electrolyte is also observed in previous research[12]. However, degradation of J_{SC} surprisingly is overcome as the $HgCl_2$ concentration increases. Only 8% degradation of J_{SC} is observed for the 6 mmol sample. This is considered to be attributed to change in chemical bonding nature of Pb-S owing to Hg^{2+} doping, which will be discussed in detail based on EXAFS analysis.

Femtosecond transient absorption (TA) spectra are measured to analyze the carrier dynamics in PbS:Hg QD-TiO_2 system along with pristine PbS QD-TiO_2 system. Fig. 2d shows femtosecond TA spectra in the near IR (NIR) region from 840 nm to 1200 nm, where the source of absorption is related to electrons in conduction band of TiO_2 [23,24]. When considering the wavelength of pump light (490 nm) which is only absorbed by the QD, NIR absorption by electrons in TiO_2 conduction band can be ascribed to the injected photoelectrons from PbS and PbS:Hg QD to TiO_2. It can be noticed that ΔO.D. increases as the $HgCl_2$ concentration increases and is highest for $HgCl_2$ concentration of 6 mmol. Since ΔO.D. is related to the injected electrons, the higher ΔO.D. is indicative of more populated electrons in TiO_2 conduction band, which is responsible not only for higher J_{SC} but also for higher V_{OC} after doping of Hg^{2+} in PbS. It is

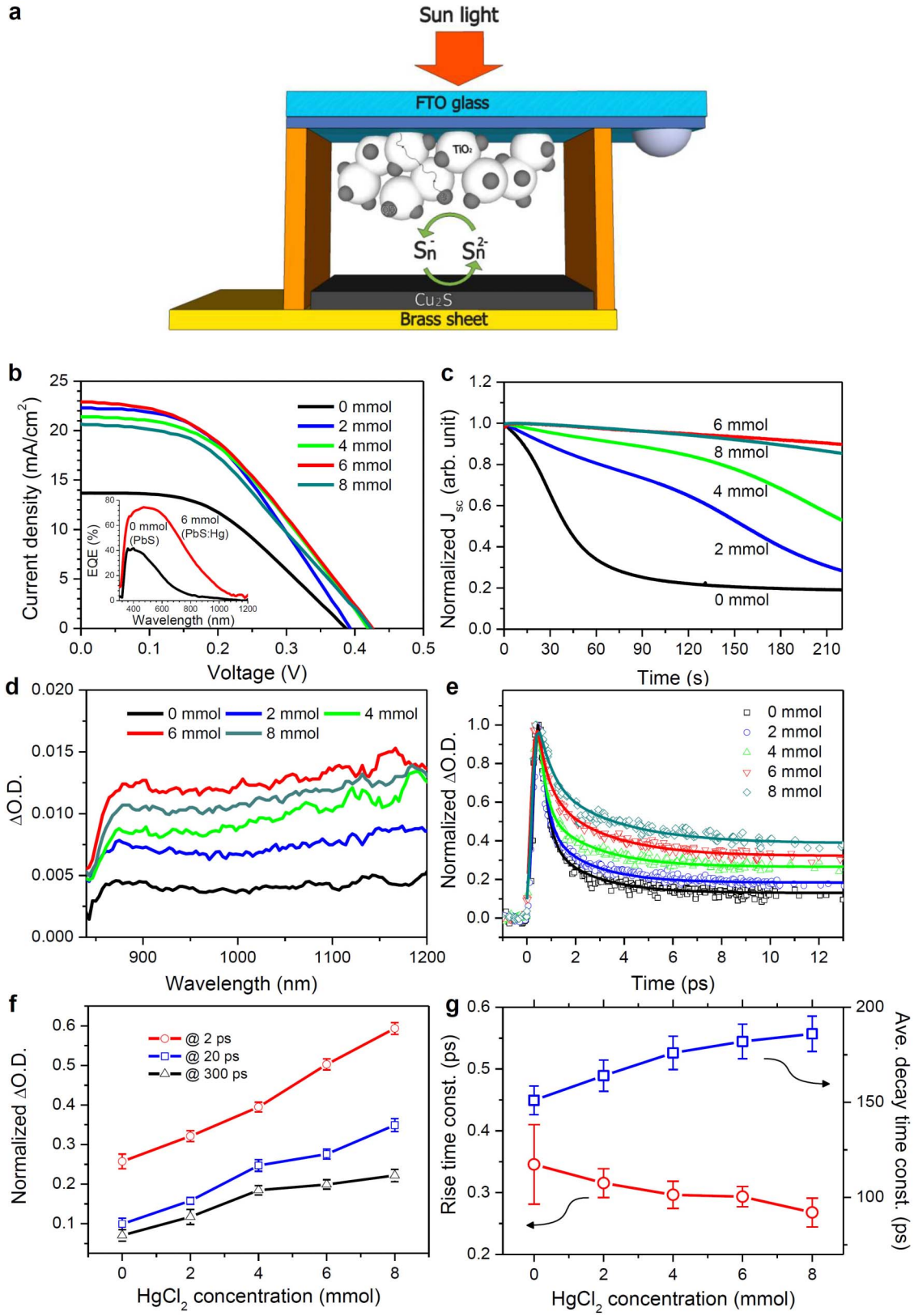

Figure 2 | Photovoltaic performance and femtosecond transient absorption spectra of PbS and PbS:Hg QDs. (a) Schematic device structure of QD-sensitized solar cell, (b) J-V curves and (c) Normalized J_{SC} as a function of time for PbS:Hg QD-sensitized solar cells with different $HgCl_2$ concentration. Inset is EQE spectra for PbS and 14.6 at% Hg^{2+} (6 mmol) doped PbS. (d) Transient absorption spectra at 0.5 ps delay. The wavelength of pump light was 490 nm. (e) Transient absorption time profile and (f) Normalized ΔOD at 2 (± 0.1) ps (red), 20 (± 1) ps (blue), and 300 (± 15) ps (black) with standard deviation. The wavelength of probe was 870 nm. (g) Intensity averaged decay time constants (blue) and rise time constants (red) with error bars.

expected that increase in ΔO.D. leads to upward shift of Fermi level, resulting in increase in V_{OC}[25]. The observed ΔO.D. is well correlated with change in V_{OC} measured in Table S4, where V_{OC} increases from 0.387 V to 0.426 V as the $HgCl_2$ increases from 0 mmol to 6 mmol and slightly decreases to 0.424 with 8 mmol. Decreased ΔO.D. for 8 mmol $HgCl_2$ condition might be related to blue shift of absorption caused by the increased band gap. TA time profile in this region exhibits triply exponential decays with an ultrafast rising component as a result of numerical convolutions with cross-correlation function (FWHM = 200 fs). In order to compare the carrier dynamics, ΔO.D. is normalized as a function of time (Fig. 2e). The decay dynamics slow down monotonically with an increased concentration of $HgCl_2$ from 0 mmol to 8 mmol. In Fig. 2f, ΔO.D. at arbitrary time delays of 2 ps, 20 ps, and 300 ps are elucidated with different $HgCl_2$ concentration. The ΔO.D. at arbitrary time increases with increased $HgCl_2$ concentration, which have the same trend with the shorter time delay (−1 ps∼13 ps). Numerically fitted parameters for decay time profile are listed in Table S6 where triply exponential model (eq 1) is used, and average decay time constants (τ_d) are estimated by eq 2[26],

$$F(t) = A_1 e^{-t/\tau_1} + A_2 e^{-t/\tau_2} + A_3 e^{-t/\tau_3} \quad (1)$$

$$\tau_d = \frac{\sum^{i=1,2,3} A_i \tau_i^2}{\sum^{i=1,2,3} A_i \tau_i} \quad (2)$$

where A_i and τ_i are triply exponential decay components constant. Average decay time constant increases from 151 ps to 186 ps as the $HgCl_2$ concentration increases from 0 mmol to 8 mmol (Fig. 2g). Absorption decay dynamics of electrons in conduction band of TiO_2 result from recombination of injected electrons with holes in QDs in absence of electrolyte. Therefore it is obvious that charge recombination in TiO_2 is substantially suppressed as the $HgCl_2$ concentration increases, which is responsible for the increased V_{OC}. Also, considering that charge collecting efficiency is inversely proportional to recombination kinetics, suppressed charge recombination may lead to improvement of charge collecting efficiency (Φ_c)[27]. Ultrafast rising of ΔO.D. signal in Fig. 2e is originated from injection of photoexcited electrons from QD to TiO_2[23,24]. Therefore, it is possible to estimate the electron injection kinetics by measuring the time for ΔO.D. signal to reach its maximum. Fitted rise time constants are listed in Table S6 and Fig. 2g. Rise time constant decreases from 340 fs to 270 fs as the $HgCl_2$ concentration increases from 0 mmol to 8 mmol, which implies an improved electron injection efficiency (Φ_{inj})[28]. It may not be ruled out that upward shift of PbS QD conduction band upon Hg^{2+} doping provides a driving force for faster electron injection in PbS:Hg QD than in PbS QD[29]. However, since the band shift of CBM of QDs seems favoring electron injection toward TiO_2, one hypothesis for the improved functional properties of the cell and the mechanism for the inhibition of charge recombination seems to be related to structural reinforcement by Hg doping.

The effect of Hg^{2+} doping on the local structure of Pb^{2+} ions in the PbS:Hg QD adsorbed on TiO_2 surface is investigated with EXAFS analysis at Pb and Hg L_3-edge. As can be seen in Fig. 3a, regardless of Hg doping, all the present PbS:Hg QDs adsorbed on TiO_2 show typical EXAFS oscillation of the reference PbS, confirming the formation of rocksalt-structured PbS phase. A closer inspection on the experimental spectra reveals that the wavelength of EXAFS oscillation becomes greater with the increase of Hg content, strongly suggesting the shortening of (Pb-S) bonds upon Hg doping[30]. The decrease of (Pb-S) bond distance upon the Hg doping is obviously verified by the quantitative EXAFS fitting analysis showing the gradual decrease of (Pb-S) distance with the increase of $HgCl_2$ concentration (Fig. 3c, Fig. 3e and Table 1). This result provides strong evidence for the reinforcement of the (Pb-S) bonds by the doping of Hg^{2+} ions. In addition to the systematic variation of bond distance, there is an overall decreasing trend of Debye-Waller factor (σ^2) with the increase of $HgCl_2$ concentration, indicating the depression of structural disorder around Pb ions (Table 1)[31]. Such a decrease of structural disorder is also attributable to the reinforcement of (Pb-S) bonds upon the Hg doping. The strengthening of chemical bonds between Pb and S leads not only to the increase of the optical band gap of PbS QD but also to the upward shift of the conduction band of PbS with antibonding character. For local structure of mercury ion, detailed analysis on the Hg L_3-edge EXAFS spectra (Fig. 3b, 3d and 3f) is performed as follows. Since the value of coordination number obtained from the EXAFS fitting analysis corresponds to the product of coordination number (CN) and amplitude reduction factor (S_0^2), it is necessary to get the knowledge of amplitude reduction factor for a Hg-S pair, prior to determining the exact coordination number of Hg ion. In the present analysis, the S_0^2 value obtained from the pure HgS reference is used to calculate the exact CN of mercury in the present PbS:Hg QDs. As listed in Table 1, this fitting analysis yields the CN of ∼3.7–4 for mercury ions in the PbS:Hg QDs, strongly suggesting the stabilization of Hg ions in the interstitial tetrahedral sites. The tetrahedral symmetry of Hg ions in the PbS:Hg QDs is further confirmed by the comparison of their bond distance with that of pure (bulk) HgS material. In comparison with the reference HgS where the Hg ions are stabilized in the tetrahedral sites with the (Hg-S) bond distance of 2.49 Å, the present PbS:Hg QDs show a shorter bond distance of ∼2.36–2.38 Å. Since the decrease of CN shortens the bond distance, the shorter (Hg-S) bond distance of the PbS:Hg QDs than that of the pure HgS underscores that the CN of Hg ion is smaller than or similar to four (i.e. the CN of Hg in the reference HgS). This result provides strong evidence for the stabilization of mercury ions in interstitial tetrahedral sites. If the Hg ions exist in octahedral symmetry (Pb site) with CN = 6, the PbS:Hg QDs should show a longer (Hg-S) bond distance than that of the reference HgS (2.49 Å) with CN = 4. The tetrahedrally coordinated interstitial Hg^{2+} ions contribute to contraction of lattice and consequently causing a reinforcement of Pb-S bond (Fig. 3g). Theoretically calculated (Hg-S) bond distance for 6 mmol $HgCl_2$ case is 2.386 Å, which is well consistent with the observed bond distance of 2.369 Å. Both the enhancement of (Pb-S) bond strength and the improvement of structural ordering around Pb^{2+} ions strongly suggest the enhanced structural stability of PbS QD via the Hg doping. In addition, the enhanced structural ordering is likely to lead to reduction of deep trap density[32,33], which contributes to suppression of charge recombination. Thus, the structural reinforcement by Hg addition is playing major role in improving the functional properties of the cell, and is the main mechanism for the inhibition of charge recombination compared to the role of band shift.

Best performance of PbS:Hg QD sensitized solar cell in this study is obtained by combination of 6 mmol $HgCl_2$ condition, scattering layer and CsOH additive in electrolyte. Addition of 0.3 M CsOH into the electrolyte improves fill factor of the device by 13% (Supplementary Fig. S10 and Table S7), which is probably due to decrease in interfacial resistance at electrolyte/Cu_2S counter electrode[34]. Light scattering layer increases further EQE at longer wavelength (EQE of 56% at 800 nm and 32% at 1000 nm). As a result, J_{SC} reaches 29.98 mA/cm², leading to a PCE as high as 5.58% at AM 1.5G one sun illumination (Fig. 4).

Discussion

We presented a mercury doped PbS QD-sensitized solar cell with extremely high J_{SC} of 30 mA/cm². Such a high J_{SC} was realized by reinforcing Pb-S bond via incorporation of Hg^{2+} ion into the interstitial site of PbS lattice. The improved ordering and covalency surrounding Pb ion led to faster electron injection and suppressed charge recombination. It is therefore concluded that structural

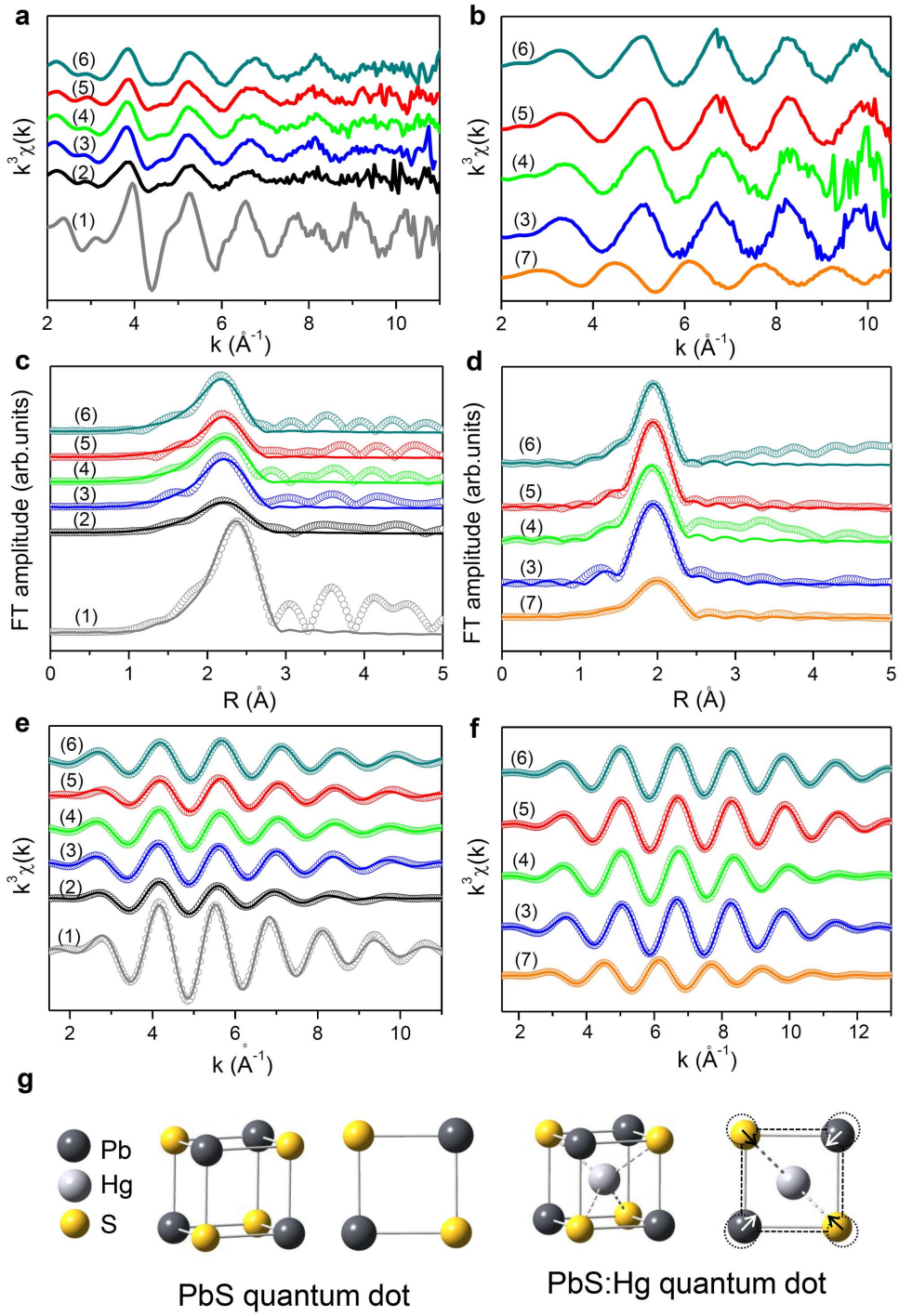

Figure 3 | Pb and Hg L_3-edge EXAFS analysis of PbS and PbS:Hg QDs. EXAFS data of Pb (a, c, e) and Hg (b, d, f) L_3-edge region. (a),(b) Experimental $k^3\chi$ (k) EXAFS oscillations, (c),(d) Fourier transformed EXAFS data, and (e)(f) the Fourier-filtered EXAFS data of (1) bulk PbS, (2) 0 mmol, (3) 2 mmol, (4) 4 mmol, (5) 6 mmol, (6) 8 mmol $HgCl_2$ and (7) bulk HgS. In the (c), (d), (e) and (f), empty circles and solid lines represent the experimental and fitted data, respectively. (g) PbS and PbS:Hg quantum dot unit cell using ball-stick model, showing contraction of Pb-S bond via interstitial occupation of Hg ion.

reinforcement by Hg addition plays a major role in improving the functional properties of the cell, and is the main mechanism for the inhibition of charge recombination. Based on our findings, optoelectronic and photovoltaic properties of QD materials are expected to be significantly improved by careful investigation on chemical bonding nature. Furthermore, such a preponderant enhancement in QD photovoltaic materials is believed to provide new insight into super high efficiency solar cell technology such as third generation MEG photovoltaics.

Methods

Sensitization of PbS:Hg QD on mesoporous TiO_2 layer. TiO_2 nanoparticles and films were prepared according to the method described elsewhere[35]. Fluorine-doped tin oxide (FTO) glass (Pilkington, TEC-8,8 Ω/sq) was cleaned with ethanol using ultrasonic cleaner for 15 min and subsequently UV/Ozone cleaning was conducted for 15 min to remove organic contaminants. A dense blocking layer was prepared on the cleaned FTO glass using 0.1 M Ti(IV) bis (ethyl acetoacetato) diisopropoxide (Aldrich, 98%) in 1-butanol (Aldrich, 99.8%) solution. TiO_2 nanoparticles were hydrothermally synthesized using titanium isopropoxide (Aldrich, 97%) in autoclave at 230°C. TiO_2 paste was prepared by mixing the synthesized nanocrystalline TiO_2, terpineol (Aldrich, 99.5%), ethyl cellulose (Aldrich, 46 cp) and lauric acid (Fluka,

Table 1 | Results of non-linear least-squares curve fitting analysis for the Pb and Hg L_3 edge spectra of the PbS and PbS:Hg QDs adsorbed on TiO_2 with different $HgCl_2$ concentration. Bulk PbS and HgS are references. CN, R and σ^2 represent coordination number, interatomic distance and Debye-Waller factor

	Bond	CN	R (Å)	$\sigma^2(10^{-3}\times Å^2)$
Bulk PbS	(Pb-S)	6	2.869	17.58
0 mmol	(Pb-S)	3.07	2.796	26.30
2 mmol	(Pb-S)	2.95	2.780	18.77
4 mmol	(Pb-S)	3.16	2.772	20.88
6 mmol	(Pb-S)	1.94	2.755	15.88
8 mmol	(Pb-S)	2.64	2.732	16.42
Bulk HgS	(Hg-S)	4	2.492	10.72
2 mmol	(Hg-S)	3.74	2.384	4.95
4 mmol	(Hg-S)	4.05	2.359	6.78
6 mmol	(Hg-S)	3.73	2.369	5.15
8 mmol	(Hg-S)	3.96	2.373	6.33

96%) with nominal composition of 1.25 : 4 : 0.3 : 0.1. The paste was further treated using three-roll-mill for 40 min to disperse nanoparticles sufficiently. The TiO_2 paste was coated on the blocking layer coated FTO substrate using doctor-blade method and annealed at 550°C for 1 h in air. Thickness of the annealed mesoporous TiO_2 layers was measured by an alpha-step IQ surface profiler (KLA Tencor). Successive ionic layer adsorption and reaction (SILAR) method was used to sensitize the TiO_2 nanoparticles with PbS:Hg QDs as described in Fig. 1a. Briefly, mesoporous TiO_2 coated electrode was first dipped in aqueous solution of 0.1 M $Pb(NO_3)_2$ (Aldrich, 99.99%) for 1 min, followed by dipped in 0.1 M Na_2S (Aldrich) for 1 min. Between each dipping, the electrode was thoroughly washed with DI (deionized) water. For PbS:Hg, 2~8 mmol of $HgCl_2$ (Sigma-Aldrich, 99.5%) was added to cationic precursor solution. These processes were defined as one cycle and several coating cycle was repeated to obtain the optimum photovoltaic performance in each condition (2 cycles for 0 mmol, 4 cycles for 2 mmol and 4 mmol and 6 cycles for 6 mmol and 8 mmol) (Supplementary Fig. S5, Fig. S6 and Table S3). To enhance the photovoltaic performance, ZnS passivation layer was deposited after PbS:Hg deposition on TiO_2 by using aqueous solution of 0.1 M $Zn(CH_3COO)_2$ (Aldrich, 99.99%) and 0.1 M Na_2S[36].

Solar cell fabrication. Cu_2S formed on a brass sheet was used for counter electrode. Brass foil (Alfa aesar, 0.25 mm thick) was etched in hydrochloric acid (SAMCHUM, 35.0~37.0%) at 80°C for 15 min and subsequently washed with DI water and dried using air gun. Polysulfide solution composed of 1 M Na_2S (Aldrich) and 1 M S (Sigma-Aldrich, 99.5%) in DI water was dropped on unmasked area of etched brass and black colored Cu_2S immediately formed on the brass foil. The PbS:Hg QD-sensitized working electrode and the Cu_2S-brass counter electrode were assembled using double-side silicon-binder-coated polyimide tape (ca. 80 μm) as a spacer and sealant. Polysulfide redox electrolyte composed of 1 M Na_2S (Aldrich) and 1 M S (Sigma-Aldrich, 99.5%) in DI water was injected through the 0.75 mm-diameter hole at working electrode and the holes were sealed using polyimide tape. For the best performance, 0.3 M of CsOH (Aldrich, 99.9%, 50 wt% solution in water) was added to electrolyte.

Materials and photovoltaic characterizations. The active area was measured by a digital microscope camera (DCMe 500) equipped with an image analysis program (Leopard 2009). Current density and voltage were measured using solar simulator (Oriel Sol 3A class AAA) equipped with 450 W Xenon lamp (Newport 6279NS) and a Keithley 2400 source meter. Light intensity was adjusted with the NREL-calibrated Si solar cell having KG-2 filter for approximating one sun light intensity (100 mW/cm^2). While measuring current and voltage, the cell was covered with an aperture mask. External quantum efficiency (EQE) was measured by a specially designed EQE system (PV measurement Inc.). A 75 W Xenon lamp (USHIO, Japan) was used as a white light source to generate monochromatic beam. Morphology and size of PbS:Hg QDs adsorbed on the nanocrystalline TiO_2 surface were investigated using a high-resolution transmission electron microscope (HR-TEM, Jeol, JEM-2100F) at an acceleration voltage of 200 kV. Average diameter of QDs was determined from TEM micrograph using image J program (version 1.45s). Stoichiometry of QDs was analyzed using X-ray photoelectron spectroscopy (VG microtech, ESCA 2000). X-ray source was Al Kα and x axis was fitted for C 1s peak to have 284.6 eV. Removal of background signal and integration of peak was conducted using VGX900-W system. Ultraviolet photoelectron spectroscopy (UPS) spectra were measured with an AXIS-NOVA using a He I (21.2 eV) gas discharge lamp. Absorbance and reflectance was measured by UV/Vis spectrometer (PerkinElmer, Lambda 1050).

Hall measurement. To prepare samples for Hall measurement, chemical bath deposition of PbS and PbS:Hg thin film was conducted as described elsewhere[37]. 1 M $Pb(CH_3COO)_2$, 1 M thiourea and 0.5 M NaOH in DI water were used for deposition of PbS while 0.85 M $Pb(CH_3COO)_2$ and 0.15 M $HgCl_2$ were used for deposition of PbS:Hg film. Both of the deposition was performed for 10 min at room temperature, which led to 300 nm thick-PbS and 235 nm thick-PbS:Hg on glass substrate. Hall voltage was measured under bias current of 1 μA for PbS film and 3 μA for PbS:Hg film, and applied field was adjusted from 1 to 5 kG using LaKeShore 7500 series Hall Measurement System at room temperature. Resistivity, type of conductivity, sheet carrier density, and mobility of majority carrier were calculated by van der Pauw method.

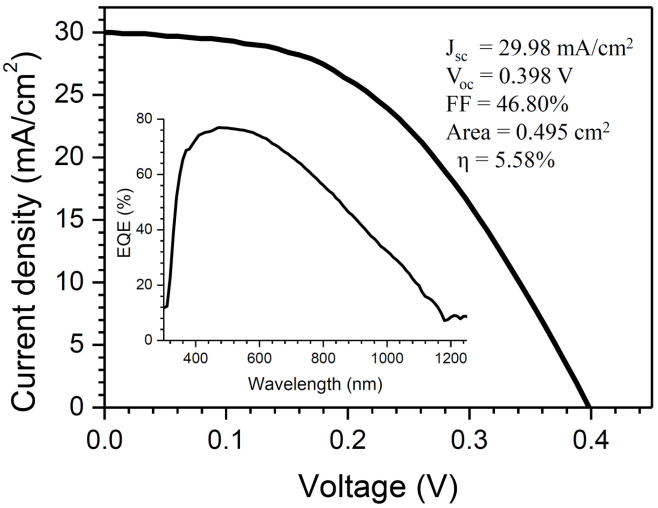

Figure 4 | Photovoltaic performance of PbS:Hg QD-sensitized solar cell. J-V curve and EQE spectrum (inset) of PbS:Hg QD-sensitized solar cell. $HgCl_2$ concentration was 6 mmol and number of coating cycle was 6. Total TiO_2 film thickness was 25 μm, comprising 5 μm with 20 nm TiO_2 particles and 20 μm with 40 nm and 500 nm TiO_2 particles.

Femtosecond transient absorption measurement. Pump-probe transient absorption (TA) experiments were carried out using commercial Helios system (Ultrafast Systmes). The pump beam of 490 nm with a pulse energy of 1.6 mJ was obtained from an optical parametric amplifier (Light conversion, TOPAS-C), pumped by a regeneratively amplified Ti:Sapphire laser system (Coherent, Libra) with 1-k Hz repetition rate. The probe pulse was a white light continuum generated by focusing a small portion of the amplifier output though a c-axis sapphire window.

XANES and EXAFS measurements. Local structure of QD was analyzed by XANES (X-ray absorption near edge structure) and EXAFS (extended X-ray absorption fine structure). The Pb L_3-edge XANES/EXAFS data were collected at room temperature in a fluorescent mode at the beam line 10C at the Pohang Accelerator Laboratory (PAL), Korea. The spectra were calibrated by measuring the spectrum of Pb foil simultaneously. Data analysis for the experimental spectra was performed with the standard procedure by using UWXAFS 2.0 program[38]. For the fitting of the reference, the amplitude reduction factor (S_0^2) was varied while the CN was fixed to the crystallographic value. All the bond distances (R), Debye-Waller factors (σ^2), and energy shifts (ΔE) were allowed to vary. In order to exactly estimate the CNs of lead ions in the present PbS:Hg QDs adsorbed on TiO_2, S_0^2 was fixed to the value from the reference PbS.

1. Nozik, A. J. *et al.* Semiconductor quantum dots and quantum dot arrays and applications of multiple exciton generation to third-generation photovoltaic solar cells. *Chem. Rev.* **110**, 6873–6889 (2010).
2. Samber, J. B., Novet, T. & Parkinson, B. A. Multiple exciton collection in a sensitized photovoltaic system. *Science* **330**, 63–66 (2010).
3. Kamat, P. V. Quantum dot solar cells. Semiconductor nanocrystals as light harvesters. *J. Phys. Chem. C* **112**, 18737–18753 (2008).
4. Tang, J. *et al.* Colloidal-quantum-dot photovoltaics using atomic-ligand passivation. *Nat. Mater.* **10**, 765–771 (2011).
5. Rühle, S., Shalom, M. & Zaban, A. Quantum-dot-sensitized solar cells. *ChemSusChem* **11**, 2290–2304 (2010).
6. Santra, P. K. & Kamat, P. V. Mn-doped quantum dot sensitized solar cells: A strategy to boost efficiency over 5%. *J. Am. Chem. Soc.* **134**, 2508–2511 (2012).
7. Pan, Z. *et al.* Highly efficient inverted type-I CdS/CdSe core/shell structure QD-sensitized solar cells. *ACS Nano* **6**, 3982–3991 (2012).
8. Kim, H.-S. *et al.* Lead iodide perovskite sensitized all-solid-state submicron thin film mesoscopic solar cell with efficiency exceeding 9%. *Sci. Rep.* **2**:**591**, 1–7 (2012).
9. Meillaud, F., Shah, A., Droz, C., Vallat-Sauvain, E. & Miazza, C. Efficiency limits for single-junction and tandem solar cells. *Sol. Energ. Mater. Sol. Cells* **90**, 2952–2959 (2006).

10. Schoolar, R. B. & Dixon, J. R. Optical constants of lead sulfide in the fundamental absorption edge region. *Phys. Rev.* **137**, A667–A670 (1965).
11. Scholes, G. D. & Rumbles, G. Excitons in nanoscale systems. *Nat. Mater.* **5**, 683–696 (2006).
12. Braga, A., Giménez, S., Concina, I., Vomiero, A. & Mora-Seró, I. Panchromatic sensitized solar cells based on metal sulfide quantum dots grown directly on nanostructured TiO_2 electrodes. *J. Phys. Chem. Lett.* **2**, 454–460 (2011).
13. Zhou, N. *et al.* Highly efficient PbS/CdS co-sensitized solar cells based on photoanodes with hierarchical pore distribution. *Electrochem. Commun.* **20**, 97–100 (2012).
14. Hyun, B.-R. *et al.* Electron injection from colloidal PbS quantum dots into titanium dioxide nanoparticles. *ACS Nano* **2**, 2206–2212 (2008).
15. Lee, H. *et al.* PbS and CdS quantum dot-sensitized solid-state solar cells: "old concepts, new results". *Adv. Funct. Mater.* **19**, 2735–2742 (2009).
16. Funasaka, K. *et al.* Detection of Pb-LIII edge XANES spectra of urban atmospheric particles combined with simple acid extraction. *Sci. Total Environ.* **403**, 230–234 (2008).
17. Zaman, K. M., Blue, L. Y., Huggins, F. E. & Atwood, D. A. Cd, Hg, and Pb compounds of benzene-1,3-diamidoethanethiol ($BDETH_2$). *Inorg. Chem.* **46**, 1975–1980 (2007).
18. Briggs, D. & Seah, M. P. *Practical Surface Analysis by Auger and X-ray photoelectron spectroscopy.* John Wiley & Sons, Chichester, UK, (1990).
19. Taniguchi, S., Green, M. & Lim, T. The room-temperature synthesis of anisotropic CdHgTe quantum dot alloys: a "molecular welding" effect. *J. Am. Chem. Soc.* **133**, 3328–3331 (2011).
20. Zhou, F., Kang, K., Maxisch, T., Ceder, G. & Morgan, D. The electronic structure and band gap of $LiFePO_4$ and $LiMnPO_4$. *Solid State Commun.* **132**, 181–186 (2004).
21. Ardalan, P. *et al.* Effects of self-assembled monolayers on solid-state CdS quantum dot sensitized solar cells. *ACS Nano* **5**, 1495–1504 (2011).
22. Carlson, B., Leschkies, K., Aydil, E. S. & Zhu, X.-Y. Valence band alignment at cadmium selenide quantum dot and zinc oxide (1010) interfaces. *J. Phys. Chem. C* **112**, 8419–8423 (2008).
23. Yoshihara, T. *et al.* Identification of reactive species in photoexcited nanocrystalline TiO_2 films by wide-wavelength-range (400–2500 nm) transient absorption spectroscopy. *J. Phys. Chem. B* **108**, 3817–3823 (2004).
24. Ellingson, R. J. *et al.* Dynamics of electron injection in nanocrystalline titanium dioxide films sensitized with $[Ru(4,4'\text{-dicarboxy-}2,2'\text{-bipyridine})_2(NCS)_2]$ by infrared transient absorption. *J. Phys. Chem. B* **102**, 6455–6458 (1998).
25. Peter, L. M. Dye-sensitized nanocrystalline solar cells. *Phys. Chem. Chem. Phys.* **9**, 2630–2642 (2007).
26. Farrow, B. & Kamat, P. V. CdSe quantum dot sensitized solar cells. shuttling electrons through stacked carbon nanocups. *J. Am. Chem. Soc.* **131**, 11124–11131 (2009).
27. Lagemaat, J. V. D., Park, N.-G. & Frank, A. J. Influence of electrical potential distribution, charge transport, and recombination on the photopotential and photocurrent conversion efficiency of dye-sensitized nanocrystalline TiO_2 solar cells: a study by electrical impedance and optical modulation techniques. *J. Phys. Chem. B* **104**, 2044–2052 (2000).
28. Cherepy, N. J., Smestad, G. P., Grätzel, M. & Zhang, J. Z. Ultrafast electron injection: implications for a photoelectrochemical cell utilizing an anthocyanin dye-sensitized TiO_2 nanocrystalline electrode. *J. Phys. Chem. B* **101**, 9342–9351 (1997).
29. Tvrdy, K., Frantsuzov, P. A. & Kamat, P. V. Photoinduced electron transfer from semiconductor quantum dots to metal oxide nanoparticles. *PNAS* **108**, 29–34 (2011).
30. Teo, B. K. *EXAFS : Basic Principles and Data Analysis.* Springer-Verlag, Berlin, (1986).
31. Tranquada, J. M. & Ingalls R. Extended x-ray-absorption fine-structure study of anharmonicity in CuBr. *Phys. Rev. B* **28**, 3520–3528 (1983).
32. Zhu, K., Vinzant, T. B., Neale, N. R. & Frank, A. J. Removing structural disorder from oriented TiO_2 nanotube arrays: reducing the dimensionality of transport and recombination in dye-Sensitized solar cells. *Nano Lett.* **7**, 3739–3746 (2007).
33. Mora-Seró, I. & Giménez, S. Recombination in quantum dot sensitized solar cells. *Accounts Chem. Res.* **42**, 1848–1857 (2009).
34. Lich, S., Tenne, R., Flaisher, H. & Manassen, J. Cation effects on the electrochemistry of anions in polysulfide photoelectrochemical cells. *J. Electrochem. Soc.* **133**, 52–59 (1986).
35. Kim, M.-J. *et al.* Unusual enhancement of photocurrent by incorporation of Brönsted base thiourea into electrolyte of dye-sensitized solar cell. *J. Phys. Chem. C* **114**, 19849–19852 (2010).
36. Guijarro, N. *et al.* Uncovering the role of ZnS treatment in the performance of quantum dot sensitized solar cells. *Phys. Chem. Chem. Phys.* **13**, 12024–12032 (2011).
37. Mane, R. S. & Lokhande, C. D. Chemical deposition method for metal chalcogenide thin films. *Mater. Chem. Phys.* **65**, 1–31 (2000).
38. Choy, J.-H., Hwang, S.-J. & Park, N.-G. Intracrystalline structure of molecular mercury halide intercalated in high-TC superconducting lattice of $Bi_2Sr_2CaCu_2O_y$. *J. Am. Chem. Soc.* **119**, 1624–1633 (1997).

Acknowledgements

This work was supported by the National Research Foundation of Korea (NRF) grant funded by the Ministry of Education, Science and Technology (MEST) of Korea under contracts No. 2012-0005601, R31-2008-10029 (WCU program) and the Global Frontier R&D Program on Center for Multiscale Energy System. J.-W.L. is grateful to global PhD fellowship grant from NRF under contract No. 2011-0008000. The experiments at Pohang Accelerator Laboratory (PAN) were supported in part by MEST and POSTECH.

Author contributions

N.-G.P. contributed to the conception and design of the experiment, analysis of the data and writing the manuscript with assistance of J.-W.L. J.-W.L. carried out design and synthesis of QD materials, preparation of the devices, device performance measurements. D.-Y.S. synthesized TiO_2 nanoparticles with different particle size. T.K.A. and H.-W.S. contributed to the femto-second data analysis. S.S. and H.H. carried out femtosecond transient measurements. M.J.K. collected UPS data. I.Y.K. and S.-J.H. measured the extended x-ray absorption fine structure (EXAFS) at PAL and analyzed the EXZFS data.

Additional information

Supplementary information accompanies this paper at http://www.nature.com/scientificreports

Competing financial interests: The authors declare no competing financial interests.

How to cite this article: Lee, J. *et al.* Quantum-Dot-Sensitized Solar Cell with Unprecedentedly High Photocurrent. *Sci. Rep.* **3**, 1050; DOI:10.1038/srep01050 (2013).